

Universal quantum reservoir computing

Sanjib Ghosh,^{1,*} Tanjung Krisnanda,¹ Tomasz Paterek,^{1,2,3} and Timothy C. H. Liew^{1,2,†}

¹*School of Physical and Mathematical Sciences,
Nanyang Technological University 637371, Singapore*

²*MajuLab, International Joint Research Unit UMI 3654,
CNRS, Université Côte d'Azur, Sorbonne Université,*

National University of Singapore, Nanyang Technological University, Singapore

³*Institute of Theoretical Physics and Astrophysics,
Faculty of Mathematics, Physics and Informatics,
University of Gdańsk, 80-308 Gdańsk, Poland*

We show that quantum reservoir neural networks offer an alternative paradigm for universal quantum computing. In this framework, a dynamical random quantum network, called the quantum reservoir, is used as a quantum processor for performing operations on computational qubits. We show various quantum operations including a universal set of quantum gates, which can be obtained with a single quantum reservoir network with different tunnelling amplitudes between the reservoir and the qubits. The same platform can also implement non-unitary quantum gates, which are useful to simulate open quantum systems with tuneable parameters. We present a comprehensive analysis of the system using the fermionic path integral formalism.

In the era of big data and machine learning, neuromorphic computing is rapidly emerging as an alternative platform for computation and data processing. While conventional computers rely on predetermined algorithms for performing tasks, neuromorphic computers use artificial neural networks, which are flexible and can learn from example in analogy to a biological brain. Their resilience allows them to be versatile in applications and adaptive to practical situations. For instance, neural networks are used across disciplines for a multitude of tasks [1–7], and are capable of extracting features from noisy [8, 9] or incomplete data [10, 11], and perturbed systems [12].

An artificial neural network is a system of interconnected nonlinear nodes capable of modelling complex mapping between input and output data. A given map is formed by carefully adjusting the connection weights between the nodes during a training procedure. While neural networks have been used for various applications, most of them are in the form of softwares implemented in conventional computers. However, hardware realizations are highly sought for exploiting the added efficiency in overcoming the so-called von Neumann bottleneck inherent in neural networks. A major challenge in hardware implementations is controlling the large number of connections between the nodes in

conventional neural network architectures [13]. Reservoir computing is an alternative architecture where the connections are taken fixed and random [14], thus avoiding the overhead of controlling a large number of connections, while keeping its wide range of applications [15, 16]. Here, the fixed random network is known as the reservoir. As it is easier to engineer a fixed and random network than a well controlled one, reservoir computing is emerging as one of most successfully implemented neural networks in a variety of physical systems [17–19]. However, most of them are working in the classical domain aiming to boost classical information processing (even using quantum reservoirs [20]). Recently, the idea of reservoir computing was brought to the quantum world for quantum information processing [21]. While some of these examples are capable of performing certain quantum information processing tasks, they are incapable of universal quantum computing.

In quantum computing, one of the most commonly used architectures is the quantum circuit model where an arbitrary quantum operation is decomposed with elementary quantum operations known as quantum gates [22]. While quantum computing has the promise to change the course of future computing, its realization requires precise engineering [23], which has led to the developments of quantum computers with only limited number of qubits so far [24, 25], while the actual number required for meaningful applications is orders of magnitude higher [26]. Currently, most hardware realizes quantum operations by applying several quantum gates in sequence. Although any quantum operation can be in principle obtained by applying gate combinations from a small set of universal quantum gates, long gate sequences require long operation time and lead to large errors. Alternatively, many frequently used elementary quantum operations can be obtained directly instead of obtaining them as combinations of a single set of universal gates. However, realising different types of operations has required different types of interaction between the qubits, which needs even more complex engineering limiting their scalability.

Here, we consider the reservoir computing framework as a basis for universal quantum computing. In reservoir computing, the reservoir is taken as a randomly connected network, which needs no optimisation itself and thus requires no precise engineering. Moreover, here we consider the connection between the nodes as basic quantum tunnelling as opposed to different types of interactions needed to achieve different quantum gates for conventional approaches. The only optimisation needed is in a control layer of connections (tunnelling amplitudes) between the qubits and the quantum reservoir, as described in Fig. 1. As opposed to conventional quantum computers, here the qubits do not interact with each other directly and are only connected via the quantum reservoir through simple quantum tunnelling. We show that a single quantum reservoir can induce

a wide variety of quantum operations on the qubits while we only control the tunnelling amplitudes to the reservoir. Moreover, we show that our scheme can directly induce non-unitary quantum operations, which can be helpful to simulate open quantum systems. Based on a fermionic path integral formalism we provide an effective picture for the dynamics of the qubits alone. This effective picture provides insight to the origin of the computational universality of our scheme.

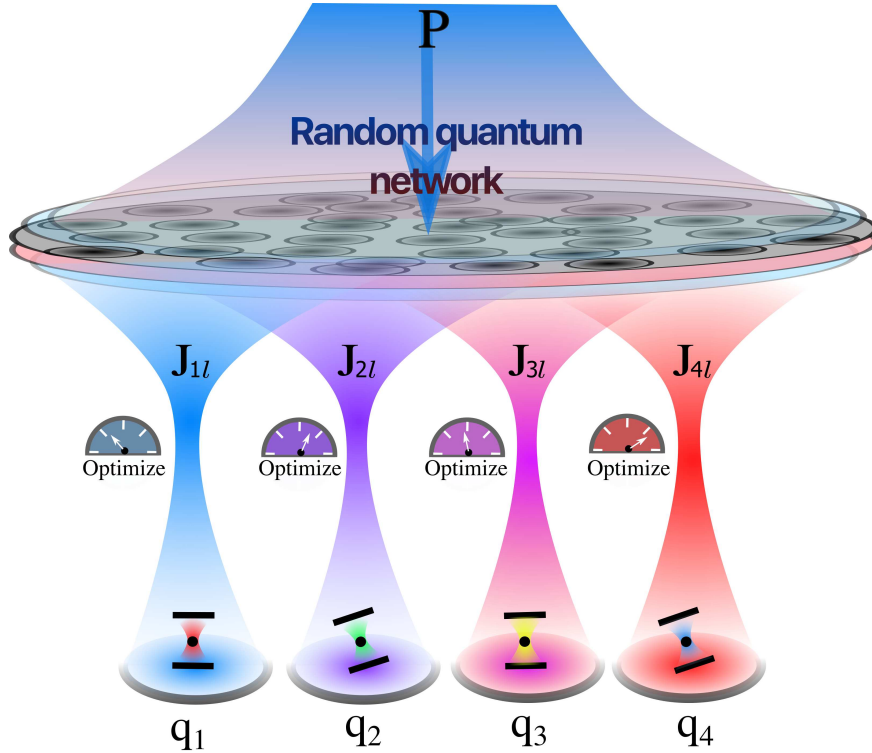


FIG. 1: The scheme for universal quantum computing based on a quantum reservoir neural network. In this framework, the network of randomly connected nodes driven with coherent excitation P is the so-called quantum reservoir. The qubits on which computation is performed are denoted by q_k . Quantum operations on qubits q_k are performed by coupling them through the reservoir. J_{kl} represent a control layer of tunnelling amplitudes connecting the qubits to the quantum network.

The model:— Our considered scheme is described in Fig. 1, where a quantum reservoir network is formed with a 2D lattice of fermions, which are interconnected via quantum tunnelling with random amplitudes and are excited with a classical field. The Fermi-Hubbard Hamiltonian representing the quantum reservoir network is given by,

$$\hat{H}_R = \sum_l E_l \hat{a}_l^\dagger \hat{a}_l + \sum_{\langle ll' \rangle} K_{ll'} (\hat{a}_l^\dagger \hat{a}_{l'} + \hat{a}_{l'}^\dagger \hat{a}_l) + \sum_l (P^* \hat{a}_l + P \hat{a}_l^\dagger), \quad (1)$$

where E_l and $K_{ll'}$ are site-dependent energies and nearest-neighbour hopping amplitudes, uniformly distributed in the intervals $[\pm E_0]$ and $[\pm K_0]$, respectively. P is the amplitude of a uniform classical optical excitation (e.g., a laser).

This fermionic network interacts with a set of qubits to realize the universal quantum processor. We consider that the qubits are independent and are connected to the quantum reservoir through quantum tunnelling with the amplitudes J_{kl} between the qubit q_k and the reservoir site l , such that the whole system is described by the Hamiltonian:

$$\hat{H} = \hat{H}_R + \sum_{kl} \left(J_{kl}^* \hat{\sigma}_k^+ \hat{a}_l + J_{kl} \hat{a}_l^\dagger \hat{\sigma}_k^- \right), \quad (2)$$

where $\hat{\sigma}_k^\pm = \hat{\sigma}_k^x \pm i\hat{\sigma}_k^y$ with $\hat{\sigma}_k^x$ and $\hat{\sigma}_k^y$ being the Pauli-X and Y operators for the qubit q_k . Note that the qubits do not directly interact with each other, but only with the quantum reservoir through quantum tunnelling. Here our proposition is to induce universal quantum operations on the qubits q_k only with suitable tunnelling amplitudes J_{kl} . The appropriate J_{kl} are obtained by training. In training, we sample a set of pure input states for the qubits and compute fidelity of the states resulting from the reservoir computing to the ideal states obtained by applying a desired quantum operation. The optimization is performed using a hybrid genetic Nelder-Mead algorithm to set the tunnelling amplitudes J_{kl} (more details are given in the Appendix). In practice, this procedure requires access to a set of ideal input-output state pairs, which can either be calculated theoretically or taken as a resource in an experimental setup. We allow J_{kl} to be complex, for generality, however this is not strictly necessary for our scheme. Once J_{kl} are optimized, the fidelity is retested with a different sample of input states.

The Fermi-Hubbard model represented by the Hamiltonian \hat{H} has efficiently been implemented using cold atoms in optical lattices [27–29] and is expected to be accessible in nonlinear cavity arrays [30, 31], depending on the strongly interacting photon regime. Substantial progress has been made toward reaching this regime using a variety of systems, including Rydberg atoms in high quality factor cavities [32], photonic crystal structures [33], superconducting circuits [34], exciton-polaritons [35], and trion-polaritons [36, 37]. A variety of physical implementations of coupling of quantum emitters to waveguides [38] or resonators [39] have also been considered, where lattices of superconducting qubits [40] have been particularly successful. These classes of systems are typically described by the Jaynes-Cummings-Hubbard model [41, 42] where bosonic cavity modes are used to couple separated fermionic modes. In the limit that the cavity mode detuning is larger than the energy exchange between the bosons and fermions, the bosonic modes can be eliminated, returning to an effective Fermi-Hubbard model [43].

Quantum operations:— Here we describe the protocol for inducing quantum operations on the qubits. An operation begins at time $t = 0$ with the initialization of qubits. We sample the initial states $|\varphi_{\text{in}}\rangle$ uniformly at random. We consider that the quantum reservoir network starts with the vacuum state $|\text{vac}\rangle_R$. The evolution of the whole system is then allowed up to a time $t = \tau$ under the classical coherent excitation represented by P and the tunnelling amplitudes J_{kl} obtained from training. We imagine that the evolution is enabled by pulses of duration τ controlling the excitation and the tunnelling amplitudes J_{kl} . The evolution of the whole system is given by the unitary operation $\hat{U} = \exp[-i\hat{H}\tau/\hbar]$. The final state of the combined system is thus given by $|\Psi_{\text{out}}\rangle = \hat{U} |\varphi_{\text{in}}\rangle \otimes |\text{vac}\rangle_R$. Although the global operation \hat{U} is unitary, the induced operation on the qubits is not necessarily unitary. This follows from the fact that during the evolution, quantum information can flow out from the qubits into the reservoir. The final state of the qubits is thus most generally represented by the density matrix $\rho_q = \text{Tr}_R[|\Psi_{\text{out}}\rangle\langle\Psi_{\text{out}}|]$ where $\text{Tr}_R[\dots]$ represents the partial trace that traces out the quantum reservoir. For each initial state we compute the fidelity given by the overlap of the ideal final quantum state $|\varphi_{\text{ideal}}\rangle = \hat{u}_q|\varphi_{\text{in}}\rangle$ and the obtained state ρ_q :

$$F = \langle\varphi_{\text{ideal}}|\rho_q|\varphi_{\text{ideal}}\rangle \quad (3)$$

where \hat{u}_q is the desired quantum operation for the qubits. We plot fidelity histograms to show that the realised gates are almost perfect for any input state.

For universal quantum computing, realizing a controlled-NOT (cNOT) gate together with certain single qubit gates is sufficient. However, here we show that the same quantum reservoir neural network can realize a range of different two-qubit gates, e.g., cNOT, controlled-Y (cY), controlled-Z (cZ) and SWAP (see Fig. 2). A specific gate operation is induced with well chosen tunnelling amplitudes J_{kl} and the pulse duration τ . In Fig. 3, we also demonstrate that high fidelity single-qubit gates are realized with a reservoir network consisting of only one node. These quantum gates and the two-qubit gates shown in Fig. 2 can perform any quantum operation.

Analysis and the effective picture:— This system is fundamentally different from the conventional schemes where operations between qubits are induced via direct interactions. Here, the interaction takes place through the quantum reservoir. Although the whole system comprising of the qubits and the quantum reservoir undergoes unitary evolution, the effective evolution of the qubits is not necessarily unitary. Here we use a path integral formalism to derive an effective picture for the qubits, which interact via the quantum network. The method follows a general prescription for a fermionic path integral given in [44, 45]. We briefly summarize the steps and results. We use Grassmann variables to express the Lagrangian of the combined system containing the reservoir

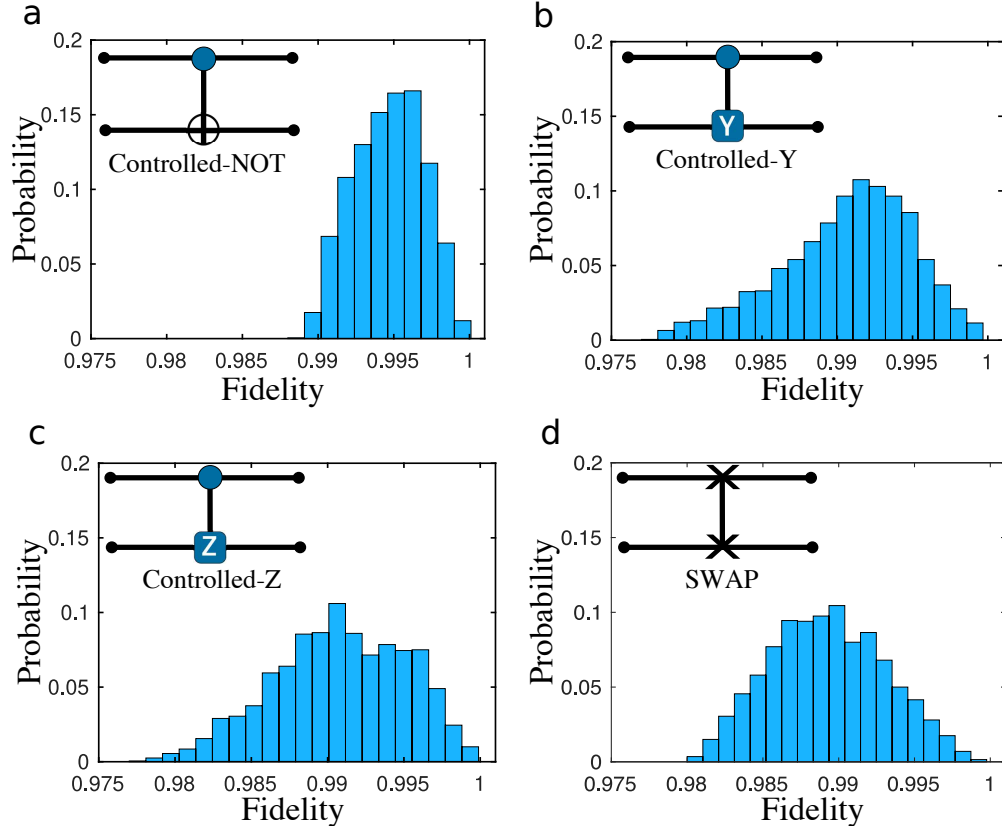


FIG. 2: Two-qubit gates and their fidelity distributions. **a**, **b**, **c**, and **d** are the fidelity distributions of the realised operations with quantum reservoir networks for cNOT, cY, cZ and SWAP as shown in the insets. Here we consider 6 fermions for the quantum reservoir. The fidelity distributions are obtained over 2000 uniformly at random generated states. The average fidelity for all gates are larger than 0.99, which is a standard parameter in process tomography. The considered parameters are presented in Table I in the Appendix.

and the qubits. It turns out that the corresponding path-integral generating function is given by Gaussian integrals. By performing the integrals using a standard technique, the reservoir is eliminated to obtain an effective action representing only the qubits. In this effective picture, the qubits are coupled to each other with their individual energies and excitations. All these effective qubit parameters are shown to be controlled by only the tunnelling amplitudes J_{kl} . Furthermore, it is shown that different single-qubit gates can be obtained in an experiment-friendly way by tuning the phase and intensity of P . Finally, this also constitutes a proof that universal quantum computing is realizable just by tuning the tunnelling couplings to the reservoir.

Here we present the derivation of the effective picture using the fermionic path integral formalism. We consider ξ_l and η_k as the Grassmann variables corresponding to the reservoir fermions \hat{a}_l and

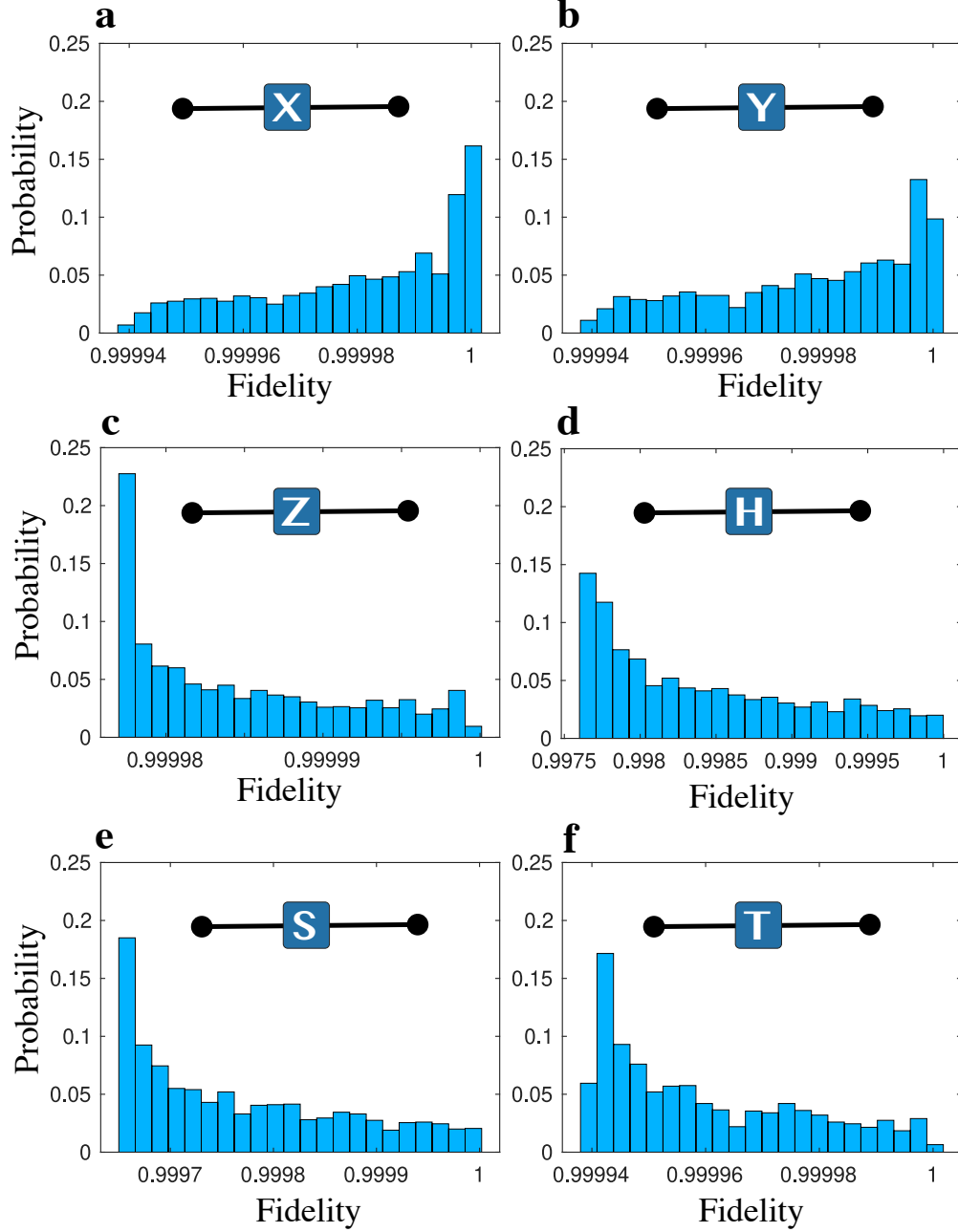


FIG. 3: Fidelities of the single-qubit gates. We show the fidelity distributions for different single-qubit gates over 2000 uniformly at random generated states. **a** to **f** show the fidelity distributions for Pauli-X, Y, Z, Hadamard, phase and $\pi/8$ gates. Here we find that a single fermionic node as the quantum reservoir is sufficient to induce the gates required for the computational universality. The average fidelity for all the single qubit gates are larger than 0.9984. The considered parameters are listed in Table II in the Appendix.

qubits σ_k , respectively. With these variables, we construct the Lagrangian for the system,

$$\mathcal{L} = i\hbar\eta^\dagger\partial_t\eta + \xi^\dagger G^{-1}\xi - \mathcal{J}^\dagger\xi - \xi^\dagger\mathcal{J}, \quad (4)$$

where the vectors $\eta = (\eta_1, \eta_2, \dots)$, $\xi = (\xi_1, \xi_2, \dots)$, $\mathcal{J} = (\mathcal{J}_1, \mathcal{J}_2, \dots)$ with $\mathcal{J}_l = \sum_k J_{kl}\eta_k + P_l$, the reservoir Green's function $G(t) = (i\hbar\partial_t - M)^{-1}$, and the matrix M is defined through the relation $M_{ll'} = E_l\delta_{ll'} + K_{ll'}$ where $\delta_{ll'}$ is the Kronecker delta function. With this action we define the path integral generating function,

$$\mathcal{Z} = \int D\eta^\dagger D\xi^\dagger D\eta D\xi e^{i\mathcal{S}}, \quad (5)$$

where the action $\mathcal{S} = \int_0^\tau \mathcal{L} dt$, and $D\lambda$ represents the functional integral of the Grassmann variable λ . We find that the functional integrals over the reservoir variables ξ_l^\dagger and ξ_l are Gaussian integrals, which we can perform with standard techniques [45]. The resultant path integral can thus be expressed only with the qubit variables:

$$\mathcal{Z} = \mathcal{Z}_0 \int D\eta^\dagger D\eta e^{i\mathcal{S}_{\text{eff}}}, \quad (6)$$

where the constant $\mathcal{Z}_0 = \exp[\text{Tr} \log(-iG^{-1})]$ and the effective action describing the qubits is given by,

$$\begin{aligned} \mathcal{S}_{\text{eff}} = \int_0^\tau dt \left[i\hbar \sum_k \eta_k^\dagger \partial_t \eta_k - \sum_k \eta_k^\dagger \mathcal{K}_k(t) \eta_k \right. \\ \left. - \sum_{k \neq k'} \eta_k^\dagger \mathcal{K}_{kk'}(t) \eta_{k'} - \sum_k \left(\mathcal{P}_k^*(t) \eta_k + \mathcal{P}_k(t) \eta_k^\dagger \right) \right] \end{aligned} \quad (7)$$

where the effective time-dependent parameters are given by,

$$\begin{aligned} \mathcal{P}_k(t) &= \sum_{l'} J_{kl}^* P_{l'} [G(t)]_{ll'}, \quad \mathcal{K}_k(t) = \sum_{l'} J_{kl}^* J_{kl'} [G(t)]_{ll'}, \\ \mathcal{K}_{kk'}(t) &= \sum_{l'} J_{kl}^* J_{k'l'} [G(t)]_{ll'}. \end{aligned} \quad (8)$$

We recognize from the effective action that $\mathcal{P}_k(t)$, $\mathcal{K}_k(t)$ and $\mathcal{K}_{kk'}(t)$ represent an effective pump (coherent driving), onsite qubit energy, and the effective hopping between two qubits k and k' , respectively. They are time dependent parameters emerging from the dynamical nature of the quantum reservoir. Importantly, these effective qubit parameters are all functions of the tunnelling couplings J_{kl} as evident in Eq. 8. This allows us to control these effective qubit parameters only through J_{kl} and thus proves the proposition that the quantum operations on the qubits can be controlled only by the tunnelling couplings J_{kl} .

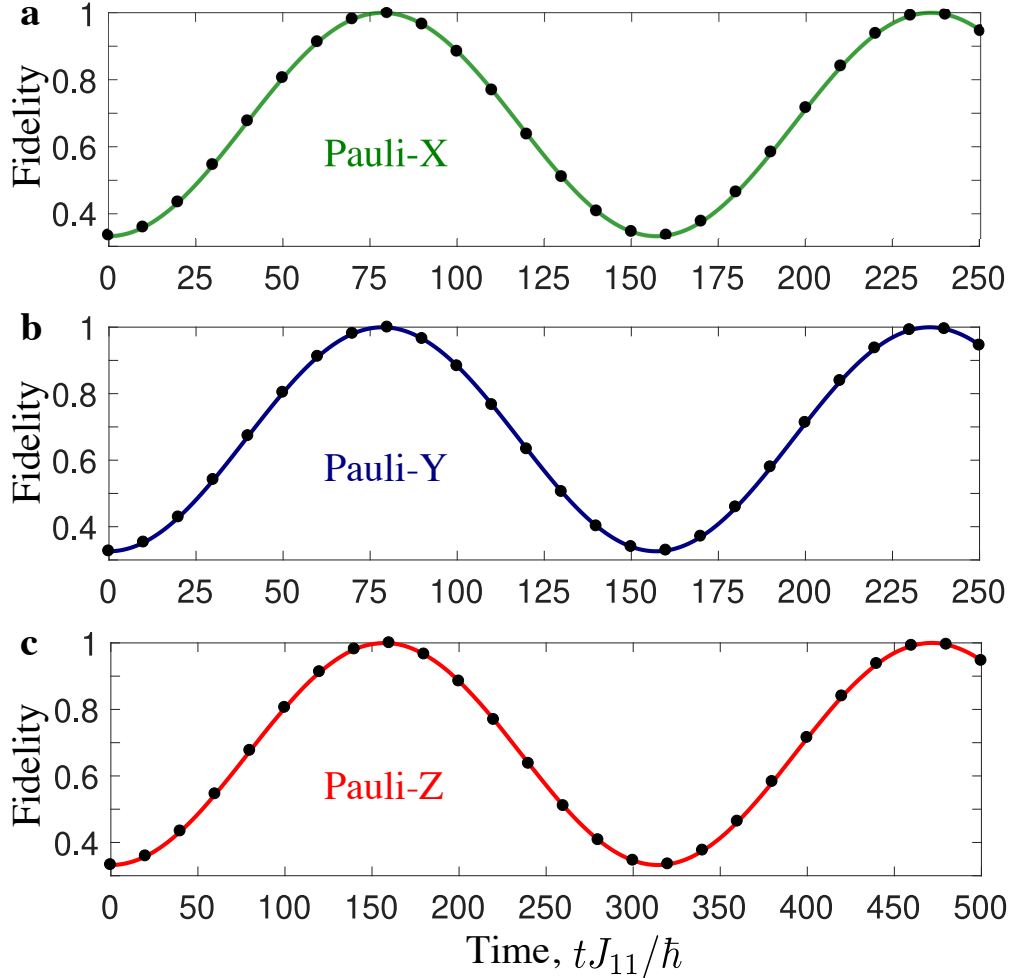


FIG. 4: Comparison between the effective theory and the exact theory. **a-c** The average fidelities as functions of time for Pauli-X,Y and Z obtained using the effective theory (points) and from the exact Hamiltonian (solid lines). The fidelities are averaged over 10^4 random initial states. We obtain high quality gates by choosing appropriate operation times where the fidelity becomes 1. Here we consider a single reservoir site connected to a qubit. The considered parameters are $P_1/J_{11} = 20, 20i$, and 0 , $E_1/J_{11} = 10^3, 10^3$, and 50 for **a-c** respectively.

Time-independent limit:— Although the effective parameters $\mathcal{P}_k(t)$, $\mathcal{K}_k(t)$ and $\mathcal{K}_{kk'}(t)$ are in general time-dependent, in the limit where the energies of the reservoir sites are much larger than any other energy scale in the system one can approximate the parameters to be time-independent. In this limit, the Green's function $G(t) \approx -M^{-1}$ (note that the matrix M consists of the reservoir

site energies and the hopping amplitudes) and thus,

$$\begin{aligned}\mathcal{P}_k &\simeq -\sum_{l'} J_{kl}^* P_{l'} M_{l'l}^{-1}, & \mathcal{K}_k &\simeq -\sum_{l'} J_{kl}^* J_{kl'} M_{l'l}^{-1} \\ \mathcal{K}_{kk'} &\simeq -\sum_{l'} J_{kl}^* J_{k'l'} M_{l'l}^{-1}\end{aligned}\quad (9)$$

In this regime, the system can be described by an effective Hamiltonian (identified from the action \mathcal{S}_{eff}):

$$\begin{aligned}\hat{H}_{\text{eff}} &= \sum_k \mathcal{K}_k \hat{\sigma}_k^z + \sum_{i \neq i'} \mathcal{K}_{kk'} (\hat{\sigma}_k^+ \hat{\sigma}_{k'}^- + \hat{\sigma}_{k'}^+ \hat{\sigma}_k^-) \\ &\quad + \sum_k (\mathcal{P}_k^* \hat{\sigma}_k^- + \mathcal{P}_k \hat{\sigma}_k^+)\end{aligned}\quad (10)$$

In Fig. 4, the comparison between the dynamics obtained from the effective Hamiltonian in Eq. 10 and the result from exact theory confirms the validity of the effective Hamiltonian picture. Note that while the validity of the effective Hamiltonian relies on the large reservoir energy compared to other energy scales, i.e., J_{kl} and P_k , the effective action given by Eq. 7 is exact. We now show how the quantum reservoir induces the universal gates in light of the effective picture.

Single-qubit gates:– The effective picture can directly explain the operating principle of the single qubit gates. With a single reservoir site, the effective Hamiltonian further simplifies to

$$\hat{H}_{\text{eff-single}} = \text{Re}[\mathcal{P}_1] \hat{\sigma}^x + \text{Im}[\mathcal{P}_1] \hat{\sigma}^y + \mathcal{K}_1 \hat{\sigma}^z \quad (11)$$

where $\mathcal{P}_1 = -J_{11}^* P_1 / E_1$, and $\mathcal{K}_1 = -|J_{11}|^2 / E_1$. Indeed such a Hamiltonian can induce any single qubit gate. In the regime $|\mathcal{K}_1 / \mathcal{P}_1| = |J_{11} / P_1| \gg 1$ where the coupling between the qubit and the reservoir site J_{11} is much larger than the pump strength P_1 , the effective Hamiltonian induces a Pauli-Z gate, which agrees exactly with our numerical finding. In the opposite regime $|\mathcal{K}_1 / \mathcal{P}_1| = |J_{11} / P_1| \ll 1$, the effective Hamiltonian induces either a Pauli-X or Y gate depending on the phase of the parameter \mathcal{P}_1 , which depends on the phase of $J_{11}^* P_1$. Note that the Hamiltonian depends on the phase of $J_{11}^* P_1$ and not individually on the phases of P_1 and J_{11} . Here we have the freedom to consider one of them constant while tuning the other one to control the Hamiltonian.

Two-qubit gates:– Realising high fidelity two-qubit gates requires multiple quantum nodes in the reservoir. The effective action describing the full dynamics is given by Eq. 7 where the two qubits interact via an effective hopping term, with effective individual energies and excitations. These effective properties of the qubits can be controlled by tuning the tunnelling couplings J_{kl} . As presented in Fig. 2, the two-qubit operations are allowed by the quantum reservoir network, which induces an effective action for the qubits given by Eq. 7. In the limit where the effective

parameters become time-independent, the dynamics of the qubits is well described by the effective Hamiltonian given by Eq. 10. Indeed this effective Hamiltonian can induce all the two-qubit gates considered in Fig. 2 when the effective parameters are appropriately chosen (details are presented in the Supplementary Information). This shows that a quantum reservoir can induce two-qubit gates, e.g., cNOT, cY, cZ and SWAP, by only controlling the tunnelling amplitudes between the qubits and the quantum reservoir.

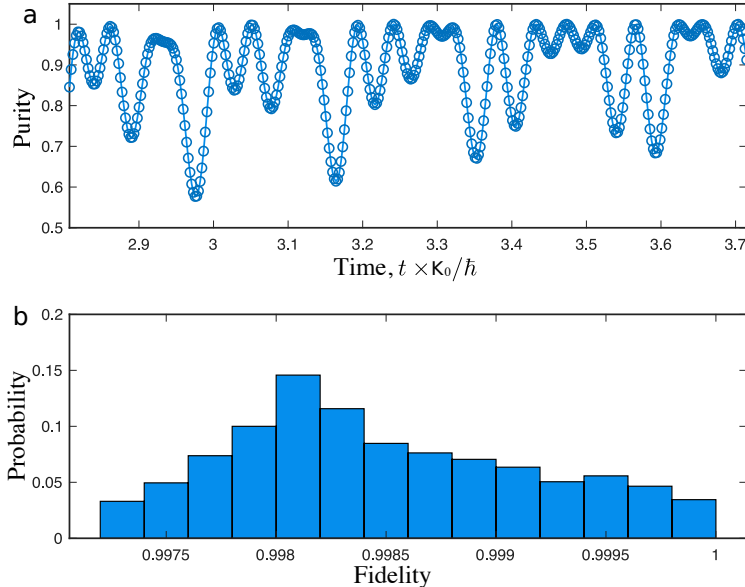


FIG. 5: A quantum reservoir can induce nonunitary operation. **a**, Purity of a qubit undergoing a quantum reservoir operation as a function of the operation time. **b**, Distribution of fidelity of a qubit evolving under a Markovian process. We consider a decay strength γ and a propagation time $t = 0.5\hbar/\gamma$ for the Markovian process. Here, we considered a single fermionic node for the reservoir and 2000 uniformly-at-random distributed initial states.

Discussion:— We have presented a platform for universal quantum computing where an underlying set of quantum nodes connects computing qubits and a learning algorithm is used to adapt the system to a particular quantum operation. Several previous works have considered how quantum neural networks can enhance the efficiency of solving classical tasks [20, 46, 47], while others have considered the use of assumed quantum computers [48–51] and quantum annealers [52] in neuromorphic architectures. In contrast, here we imagine a neuromorphic architecture that can allow a set of quantum nodes to realize universal quantum computation. The learning of quantum operations from quantum networks has been considered before, based on nonlocal spin coupling [53] and adiabatic pulse control [54]. The advantage of the reservoir network architecture introduced here is that only quantum tunnelling is considered for network connections, which is readily acces-

sible in many systems (e.g. photonics, polaritons, cold atoms, and trapped ions), and, that only a small subset of total network connection weights need to be controlled. We note that a very simple learning algorithm in the optimization of the tunnelling amplitudes was used. The application of more advanced evolutionary algorithms in quantum control would likely lead to improved results for our system [55].

In general, the operations induced by the quantum reservoir on the qubits are nonunitary in nature. The signature of the nonunitary nature of the operation can be observed in the purity of the qubits. In Fig. 5 **a**, we show the purity of a qubit undergoing a quantum reservoir operation as a function of operation time. We find that the purity of the qubit oscillates and reaches 1 only at certain times. The effective operation on the qubit is thus unitary only at those times. The system can therefore implement non-unitary gates. For a demonstration we consider a Markovian dynamics for the qubit given by the master equation: $\hbar\dot{\rho} = (\gamma/2)(2\sigma^- \rho \sigma^+ - \sigma^+ \sigma^- \rho - \rho \sigma^+ \sigma^-)$. Using the quantum reservoir, we obtain a non-unitary quantum operation equivalent to the same induced by the master equation of the qubit. In Fig. 5 **b**, we show the fidelity between the quantum states obtained from quantum reservoir processing and from solving the quantum master equation.

APPENDIX

Grassmann variable

A Grassmann variable λ satisfies $\lambda^2 = 0$. A general function $f(\lambda)$ can be written as $f(\lambda) = c_0 + c_1\lambda$ as the higher power terms will be zero due to the property $\lambda^2 = 0$ (here c_0 and c_1 are ordinary numbers). An integral should satisfy,

$$\int d\lambda f(\lambda) = \int d\lambda f(\lambda + \lambda') \quad (12)$$

where the integrals are performed in the whole space, and we made a change of variable $\lambda \rightarrow \lambda + \lambda'$ with λ' being a Grassmann constant. From this relation we find the integral properties: $\int d\lambda = 0$ and $\int \lambda d\lambda = 1$.

The equations of motion can be obtained from the Euler-Lagrange equation:

$$\frac{\partial \mathcal{L}}{\partial \lambda} = \partial_t \frac{\partial \mathcal{L}}{\partial (\partial_t \lambda)} \quad (13)$$

which are identified to the Schrödinger equations for the fermionic field λ and the Lagrangian \mathcal{L} .

Here we present the Gaussian path integrals used for obtaining the effective picture for the

qubits only. In the path integral formalism, a generating function for a field λ is defined as,

$$\int D\lambda^\dagger D\lambda e^{i \int_0^\tau dt [ih\lambda^\dagger \partial_t \lambda - H(\lambda^\dagger, \lambda) + \lambda^\dagger P + P^\dagger \lambda]} \quad (14)$$

where $D\lambda$ (and $D\lambda^\dagger$) is the path integral for the Grassmann variable λ (and λ^\dagger), P represents a source term (pump), and $H(\lambda^\dagger, \lambda)$ is the Hamiltonian function. For evaluating the Gaussian path integrals, we use the relation:

$$\int D\lambda^\dagger D\lambda e^{-\lambda^\dagger \mathbf{A} \lambda} = \det[\mathbf{A}] = \exp[\text{Tr}(\log \mathbf{A})] \quad (15)$$

where \mathbf{A} is a matrix, $\det[\mathbf{A}]$ is its determinant. Also,

$$\int D\lambda^\dagger D\lambda e^{-\lambda^\dagger \mathbf{A} \lambda - \lambda^\dagger B - B^\dagger \lambda} = \det[\mathbf{A}] e^{B^\dagger \mathbf{A}^{-1} B} \quad (16)$$

where \mathbf{A}^{-1} is the inverse of the matrix \mathbf{A} and B is a vector representing a source term.

Training

One of the main features of neural network frameworks is that they learn from examples without being told the specific rules of the task. Here we take advantage of this powerful feature and use it for realizing various quantum operations by training the quantum reservoir network. While in conventional approaches, different quantum gate operations require realizing different types of interactions between the qubits, here, the same quantum network is used to obtain different operations. Given a quantum operation \hat{u}_q , that we want to realize, we consider a set of example quantum states $|\varphi_{\text{in}}^{(j)}\rangle$ for the qubits for training. For each example quantum state $|\varphi_{\text{in}}^{(j)}\rangle$, we calculate the fidelity F_j given by Eq. 3. We numerically maximize the average fidelity

$$\bar{F} = \frac{1}{N} \sum_{j=1}^N F_j \quad (17)$$

with optimal choice of tunnelling amplitudes J_{kl} , where N is the number of quantum states in the training set. We empirically find that for two-qubit gate operation 10 randomly generated quantum states are sufficient for training.

Training of the quantum neural network is an optimization process. The average fidelity $\bar{F}(J_{kl})$ is a nonlinear function of the tunnelling amplitudes J_{kl} . For a small number of parameters J_{kl} , a deterministic method such as the Nelder-Mead simplex algorithm is sufficient to achieve the optimum condition. However, for large numbers of J_{kl} , we use a stochastic genetic algorithm to

Gate	E_0/K_0	P/K_0	$\tau K_0/\hbar$
cNOT	1	400	0.15
cY	1	400	0.135
cZ	1	154	0.15
SWAP	2	5.5	0.2

TABLE I: Parameters considered to obtain two-qubit gates. These gates are obtained with a quantum reservoir of 6 sites.

find the optimum condition starting from a set of initial guesses, which approach the optimum point in a random process.

Genetic algorithms are inspired by the biological evolution based on natural selection. The process starts with a random set of populations that goes through a natural selection procedure based on a fitness criterion. The fittest individuals reproduce the next generation of populations through a cross breeding procedure. Random mutation in the new generation ensures diversity among the populations.

Here, J_{kl} with all k and l represent one individual in a genetic algorithm. We define a population with a set of M such individuals J_{kl}^m where $m = 1, 2 \dots M$. We start with a random choice of population. The fitness criterion is defined through calculating the average fidelity $\bar{F}(J_{kl}^m)$ for an individual m .

The next generation of population is reproduced by the two individuals with largest average fidelities, keeping the total population size fixed to M . The next generation $J_{kl}'^m$ is born with the cross breeding rule:

$$J_{kl}'^m = (J_{kl}^p + J_{kl}^q)/2 + \delta f_{\text{ran}} \quad (18)$$

where δ and f_{ran} represent a mutation rate and a Gaussian random number, respectively. The process of natural selection is then repeated for the new generation until the optimum condition is found.

Parameters:— The considered parameters for obtaining the quantum gate operations are noted in tables I and II.

One-qubit gates

The setup:— Here we consider a special case where one input qubit interacts with a one-site reservoir (a fermion). The reservoir has an onsite energy E_1 , a coherent driving (pump) P , and

Gate	E_0/K_0	P/K_0	$\tau K_0/\hbar$	Gate	E_0/K_0	P/K_0	$\tau K_0/\hbar$
X	1	60	2.032	H	1	4.96	1
Y	1	60	11	S	1	0.1	2.02
Z	1	0.1	4.14	T	1	0.1	3.11

TABLE II: Parameters considered to obtain single-qubit quantum gates. The single-qubit gates are obtained with a single reservoir site.

negligible decay. The dynamics of the whole system is unitary, where the Hamiltonian is written as

$$H = E_1 \hat{a}_1^\dagger \hat{a}_1 + P \hat{a}_1^\dagger + P^* \hat{a}_1 + J_{11} (\hat{\sigma}_1^+ \hat{a}_1 + \hat{a}_1^\dagger \hat{\sigma}_1^-), \quad (19)$$

with J_{11} being the strength of the coupling term. Note that we have used $\hat{\sigma}_1^-$ (\hat{a}_1) as the annihilation operator of the input qubit (the reservoir site). Below we will present the working parameters for the dynamics of this system such that the evolution of the input qubit implements the X, Y, and Z gates given by the Pauli operators

$$\hat{\sigma}^x = \begin{pmatrix} 0 & 1 \\ 1 & 0 \end{pmatrix}, \quad \hat{\sigma}^y = \begin{pmatrix} 0 & -i \\ i & 0 \end{pmatrix}, \quad \hat{\sigma}^z = \begin{pmatrix} 1 & 0 \\ 0 & -1 \end{pmatrix}, \quad (20)$$

respectively. We will present two regimes, namely the low and high reservoir energy limit, in which one can implement the one-qubit gates on the input qubit.

Low energy limit ($E_1 \ll |P|, J_{11}$):— First of all, note that the most important component in the system is given by the hopping interaction between the input qubit and the reservoir. In particular, if one were to consider this term alone, the eigenstates and eigenvalues are given by $\{|00\rangle, |11\rangle, |\psi_-\rangle, |\psi_+\rangle\}$ and $\{0, 0, -J_{11}, J_{11}\}$, respectively. We have used the Bell-state notation $|\psi_\pm\rangle = (|01\rangle \pm |10\rangle)/\sqrt{2}$. Therefore, one can see that, in the case of $E_1 = |P| = 0$, the evolution of the system follows $\hat{U}(t) = |00\rangle\langle 00| + |11\rangle\langle 11| + \exp(iJ_{11}t/\hbar)|\psi_-\rangle\langle\psi_-| + \exp(-iJ_{11}t/\hbar)|\psi_+\rangle\langle\psi_+|$, which, at $J_{11}\tau/\hbar = \pi + 2\pi n$, reduces to

$$\hat{U}(\tau) = \hat{\sigma}_q^z \otimes \hat{\sigma}_r^z, \quad (21)$$

where the subscript q (r) denotes the input qubit (the reservoir). This evolution executes the Z gate on the input qubit.

For the implementation of the X and Y gates, let us first note that if we consider only the pumping term of the reservoir, one can either have $H \propto \hat{\sigma}_r^x$ when the pump P is real or $H \propto \hat{\sigma}_r^y$ when the pump has a phase, in particular, $P = |P| \exp(\pm i\pi/2)$. This allows the application of either the X or Y gate on the state of the reservoir at $|P|\tau/\hbar = \pi/2 + \pi n$. In order to implement the

gates on the state of the input qubit, let us consider the interaction J_{11} in addition to the reservoir pumping term, and also assume the strength $|P| \gg J_{11}$. In this limit, one can confirm that the evolution operator of the system, at time $J_{11}\tau/\hbar = \pi + 2\pi n$, where $n = 0, 1, 2, \dots$, is given by

$$\hat{U}(\tau) = e^{-i(\pi/2+\pi n)} \hat{\sigma}_q^x \otimes \hat{\sigma}_r^x, \quad (22)$$

$$\hat{U}(\tau) = e^{-i(\pi/2+\pi n)} \hat{\sigma}_q^y \otimes \hat{\sigma}_r^y, \quad (23)$$

if P is real and $P = |P| \exp(\pm i\pi/2)$ is imaginary, respectively. These evolution operators realise the X (Eq. 22) and Y (Eq. 23) gates. Furthermore, the addition of the onsite energy, with $E_1 \ll |P|$, does not change the conclusion as it simply adds an overall phase to the gate.

In order to have control over the application of the gates above, one can consider a system in a regime where $|P| \gg J_{11} \gg E_1$. It is apparent that in this way, one can control (to some extent) or switch the gates by changing the pumping strength of the reservoir. In particular, the Z gate is realised when $P = 0$ (still in the regime $J_{11} \gg E_1$) whereas the X and Y gates are realised by having real P and imaginary $P = |P| \exp(\pm i\pi/2)$, respectively. We note again that all the gates are achieved at $J_{11}\tau/\hbar = \pi + 2\pi n$.

High energy limit ($E_1 \gg |P|, J_{11}$):— Now we present another set of working parameters in the limit where the energy of the reservoir site is much higher than the pumping and interaction terms, as illustrated in the main text. In this limit, one can simplify the expression of the unitary operator for the application of the X, Y, and Z gates.

The Z gate can be achieved without pumping. At times $J_{11}^2\tau/(E_1\hbar) = \pi + 2\pi n$, the evolution operator reduces to the expression written in Eq. (21). On the other hand, one can achieve the X and Y gates by taking $|P| \gg J_{11}$. Indeed, one can confirm that the evolution at times $J_{11}P\tau/(E_1\hbar) = \pi/2 + \pi n$ follows

$$\hat{U}(\tau) = -e^{-i(\pi/2+\pi n)} \hat{\sigma}_q^x \otimes \hat{\sigma}_r^z, \quad (24)$$

$$\hat{U}(\tau) = \mp e^{-i(\pi/2+\pi n)} \hat{\sigma}_q^y \otimes \hat{\sigma}_r^z, \quad (25)$$

for real P and $P = |P| \exp(\pm i\pi/2)$, respectively.

High energy limit and effective picture:— In the main text we have shown that the effective picture is indeed confirmed by numerical results from the dynamics of the bipartite Hamiltonian of Eq. (19). In particular, both methods are shown to be in agreement in the high energy limit, as can be seen in Fig. 4 of the main text. For completeness, here we present other sets of parameters in which one can see when the approximations used start to show some difference, cf. Fig. 6. One

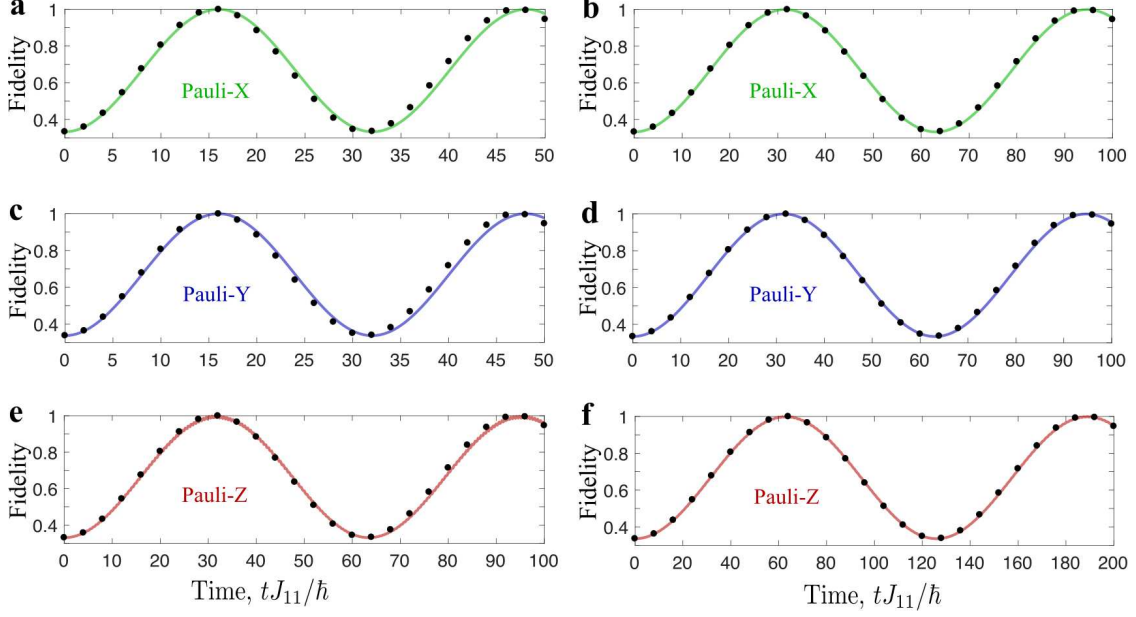


FIG. 6: Fidelity dynamics of one-qubit X, Y, and Z gates. Panels **a** and **b** show the X-gate fidelity with $E_1/J_{11} = 200$ and $E_1/J_{11} = 400$, respectively. The pumping is taken to be the same, i.e., $P/J_{11} = 20$. The Y-gate fidelity is plotted with similar parameters as the X gate, where now $P/J_{11} = 20 \exp(i\pi/2)$. The corresponding results are illustrated in panels **c** and **d**. Panels **e** and **f** depict the dynamics of the Z-gate fidelity with $E_1/J_{11} = 10$ and $E_1/J_{11} = 20$, respectively. In this case, the pumping is not required. The fidelity in all the panels is averaged over 10^4 random initial states of the input qubit.

can see that the two methods are coinciding nicer for higher energy ratio, i.e., panels **b**, **d**, and **f** in Fig. 6.

Two-qubit gates (via direct interactions)

The setup:— Consider two interacting two-level systems as in the effective picture discussed in the main text. Each qubit has an onsite energy E_j , a coherent pumping P_j , and no decay. Together with a hopping interaction term, one writes the Hamiltonian as

$$H = \sum_{j=\{1,2\}} E_j \hat{a}_j^\dagger \hat{a}_j + P_j \hat{a}_j^\dagger + P_j^* \hat{a}_j + J(\hat{a}_1 \hat{a}_2^\dagger + \hat{a}_2 \hat{a}_1^\dagger). \quad (26)$$

It will be shown below that this type of system is able to implement universal two-qubit gates on its initial state. We will start by presenting the working parameters for important gates, such as the square-root-swap (sSWAP), control-X (cNOT), control-Y (cY), control-Z (cZ), square-root-iSwap

(siSWAP), and swap (SWAP). These gates are written as

$$\begin{aligned}
 & \frac{1}{2} \begin{pmatrix} 2 & 0 & 0 & 0 \\ 0 & (1+i) & (1-i) & 0 \\ 0 & (1-i) & (1+i) & 0 \\ 0 & 0 & 0 & 2 \end{pmatrix}, \begin{pmatrix} 1 & 0 & 0 & 0 \\ 0 & 1 & 0 & 0 \\ 0 & 0 & 0 & 1 \\ 0 & 0 & 1 & 0 \end{pmatrix}, \\
 & \begin{pmatrix} 1 & 0 & 0 & 0 \\ 0 & 1 & 0 & 0 \\ 0 & 0 & 0 & -i \\ 0 & 0 & i & 0 \end{pmatrix}, \begin{pmatrix} 1 & 0 & 0 & 0 \\ 0 & 1 & 0 & 0 \\ 0 & 0 & 1 & 0 \\ 0 & 0 & 0 & -1 \end{pmatrix}, \\
 & \frac{1}{\sqrt{2}} \begin{pmatrix} \sqrt{2} & 0 & 0 & 0 \\ 0 & 1 & i & 0 \\ 0 & i & 1 & 0 \\ 0 & 0 & 0 & \sqrt{2} \end{pmatrix}, \begin{pmatrix} 1 & 0 & 0 & 0 \\ 0 & 0 & 1 & 0 \\ 0 & 1 & 0 & 0 \\ 0 & 0 & 0 & 1 \end{pmatrix}, \tag{27}
 \end{aligned}$$

respectively.

Simulations:— We performed a search algorithm realising the above two-qubit gates. Our numerical results show that all these gates can be achieved with gate fidelity $\bar{F} > 0.999$, see Table III for exemplary parameters. See Fig. 7 for a comparison of the high fidelity achieved with the search method for different gates. Note that genetic algorithms have been used for realising \hat{U}_{sSWAP} , \hat{U}_{cNOT} , \hat{U}_{cY} , and \hat{U}_{cZ} . The parameters for \hat{U}_{siSWAP} and \hat{U}_{sSWAP} are not sensitive to small changes and therefore we did not perform precise search algorithms.

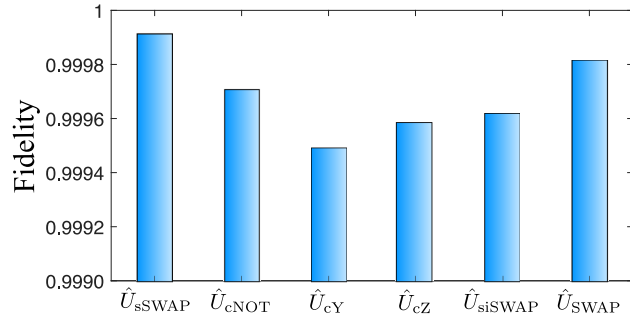


FIG. 7: Fidelity \bar{F} of various two-qubit gates for the parameters listed in Table III.

Universality:— We note that each of the two-qubit gates presented above, apart from the SWAP gate, combined with single-qubit gates form a universal set. In this way, they are equivalent to each other. As an example, we recall that the cNOT gate can be created, by the cY, cZ, sSWAP

TABLE III: Exemplary parameters for the realisation of two-qubit gates. We have used $\tau = E_2 t / \hbar$. All the gates are achieved with $\bar{F} > 0.999$ with $N = 10^5$. Note that the parameters for the \hat{U}_{siSWAP} and \hat{U}_{SWAP} gates are not as sensitive as the others. Especially for \hat{U}_{siSWAP} , one gets very high fidelity in the limit $E_1 = E_2 \gg P_1 = P_2, J$.

Two-qubit	Parameters				
Gates	E_1/E_2	P_1/E_2	P_2/E_2	J/E_2	τ
\hat{U}_{sSWAP}	0.923091	5.158696	5.155802	0.937275	48.168039
\hat{U}_{cNOT}	140.703597	0.958346	140.627941	2.826258	40.303524
\hat{U}_{cY}	138.217022	$-0.089054 - 0.920161i$	$0.079873 - 138.295970i$	2.881602	40.778441
\hat{U}_{cZ}	1.006724	1.094922	0.932635	117.958714	45.402586
\hat{U}_{siSWAP}	1	0.01	0.01	0.01	1181
\hat{U}_{SWAP}	1	1.5	1.5	42.8	37.6

or siSWAP gate with the help of single qubit gates as follows

$$\begin{aligned}
\hat{U}_{\text{cNOT}} &= [\mathbb{1} \otimes \hat{R}_z(-\pi/2)] \hat{U}_{\text{cY}} [\mathbb{1} \otimes \hat{R}_z(\pi/2)], \\
\hat{U}_{\text{cNOT}} &= [\mathbb{1} \otimes \hat{R}_y(\pi/2)] \hat{U}_{\text{cZ}} [\mathbb{1} \otimes \hat{R}_y(-\pi/2)], \\
\hat{U}_{\text{cNOT}} &= [\mathbb{1} \otimes \hat{R}_y(-\pi/2)] \hat{U}_{\text{sSWAP}} [\hat{Z} \otimes \mathbb{1}] \hat{U}_{\text{sSWAP}} \\
&\quad [\hat{R}_z(-\pi/2) \otimes \hat{R}_z(-\pi/2)] [\mathbb{1} \otimes \hat{R}_y(\pi/2)], \\
\hat{U}_{\text{cNOT}} &= [\hat{X} \otimes \hat{X}] [\hat{R}_y(-\pi/2) \otimes \mathbb{1}] \\
&\quad [\hat{R}_x(\pi/2) \otimes \hat{R}_x(-\pi/2)] \hat{U}_{\text{siSWAP}} [\hat{R}_x(\pi) \otimes \mathbb{1}] \\
&\quad \hat{U}_{\text{siSWAP}} [\hat{R}_y(\pi/2) \otimes \mathbb{1}] [\hat{Z} \otimes \mathbb{1}] [\hat{X} \otimes \hat{X}] e^{i\pi/4}.
\end{aligned} \tag{28}$$

Note that we have used the following single-qubit rotation matrices.

$$\begin{aligned}
\hat{R}_x(\alpha) &= \begin{pmatrix} \cos(\frac{\alpha}{2}) & -i \sin(\frac{\alpha}{2}) \\ -i \sin(\frac{\alpha}{2}) & \cos(\frac{\alpha}{2}) \end{pmatrix}, \quad \hat{R}_z(\delta) = \begin{pmatrix} 1 & 0 \\ 0 & e^{i\delta} \end{pmatrix}, \\
\hat{R}_y(\beta) &= \begin{pmatrix} \cos(\frac{\beta}{2}) & -\sin(\frac{\beta}{2}) \\ \sin(\frac{\beta}{2}) & \cos(\frac{\beta}{2}) \end{pmatrix}.
\end{aligned} \tag{29}$$

Even though different gates can be constructed from specific combinations of a universal set of gates, it should be noted that the ability to directly construct the gate needed for a particular application will bring the highest efficiency in terms of operation time. Indeed the ability of the quantum reservoir neural network to learn to perform a whole range of different quantum gates is one of its advantages.

ACKNOWLEDGMENTS

SG, TK and TL were supported by the Ministry of Education (Singapore), grant no: MOE2017-T2-1-001. TP acknowledges Polish National Agency for Academic Exchange NAWA Project No. PPN/PPO/2018/1/00007/U/00001.

* Electronic address: sanjib.ghosh@ntu.edu.sg

† Electronic address: timothyliew@ntu.edu.sg

- [1] Webb, S. Deep learning for biology. *Nature* **554**, 555–557 (2018).
- [2] Jones, D. T. Setting the standards for machine learning in biology. *Nature Reviews Molecular Cell Biology* **20**, 659–660 (2019). URL <https://doi.org/10.1038/s41580-019-0176-5>.
- [3] Topol, E. J. High-performance medicine: the convergence of human and artificial intelligence. *Nature Medicine* **25**, 44–56 (2019). URL <https://doi.org/10.1038/s41591-018-0300-7>.
- [4] Hannun, A. Y. *et al.* Cardiologist-level arrhythmia detection and classification in ambulatory electrocardiograms using a deep neural network. *Nature Medicine* **25**, 65–69 (2019). URL <https://doi.org/10.1038/s41591-018-0268-3>.
- [5] Nagy, A. & Savona, V. Variational quantum monte carlo method with a neural-network ansatz for open quantum systems. *Physical Review Letters* **122**, 250501– (2019). URL <https://link.aps.org/doi/10.1103/PhysRevLett.122.250501>.
- [6] Vicentini, F., Biella, A., Regnault, N. & Ciuti, C. Variational neural-network ansatz for steady states in open quantum systems. *Physical Review Letters* **122**, 250503– (2019). URL <https://link.aps.org/doi/10.1103/PhysRevLett.122.250503>.
- [7] Mehta, P. *et al.* A high-bias, low-variance introduction to machine learning for physicists. *Physics Reports* **810**, 1–124 (2019). URL <http://www.sciencedirect.com/science/article/pii/S0370157319300766>.
- [8] Wong, K. Y. M. & Sherrington, D. Neural networks optimally trained with noisy data. *Physical Review E* **47**, 4465–4482 (1993). URL <https://link.aps.org/doi/10.1103/PhysRevE.47.4465>.
- [9] Borodinov, N. *et al.* Deep neural networks for understanding noisy data applied to physical property extraction in scanning probe microscopy. *npj Computational Materials* **5**, 25 (2019). URL <https://doi.org/10.1038/s41524-019-0148-5>.
- [10] Che, Z., Purushotham, S., Cho, K., Sontag, D. & Liu, Y. Recurrent neural networks for multivariate time series with missing values. *Scientific Reports* **8**, 6085 (2018). URL <https://doi.org/10.1038/s41598-018-24271-9>.
- [11] Ding, G., Liu, Y., Zhang, R. & Xin, H. L. A joint deep learning model to recover information and reduce artifacts in missing-wedge sinograms for electron tomography and beyond. *Scientific Reports* **9**,

- 12803 (2019). URL <https://doi.org/10.1038/s41598-019-49267-x>.
- [12] Ming, Y., Lin, C.-T., Bartlett, S. D. & Zhang, W.-W. Quantum topology identification with deep neural networks and quantum walks. *npj Computational Materials* **5**, 88 (2019). URL <https://doi.org/10.1038/s41524-019-0224-x>.
- [13] Roy, K., Jaiswal, A. & Panda, P. Towards spike-based machine intelligence with neuromorphic computing. *Nature* **575**, 607–617 (2019). URL <https://doi.org/10.1038/s41586-019-1677-2>.
- [14] Lukoševičius, M. *A Practical Guide to Applying Echo State Networks*. Neural Networks: Tricks of the Trade (Springer, Berlin, Heidelberg, 2012), 2 edn. URL https://doi.org/10.1007/978-3-642-35289-8_36.
- [15] Grigoryeva, L. & Ortega, J.-P. Echo state networks are universal. *Neural Networks* **108**, 495–508 (2018). URL <http://www.sciencedirect.com/science/article/pii/S089360801830251X>.
- [16] Seoane, L. F. Evolutionary aspects of reservoir computing. *Philosophical Transactions of the Royal Society B: Biological Sciences* **374**, 20180377 (2019). URL <https://doi.org/10.1098/rstb.2018.0377>.
- [17] Tanaka, G. *et al.* Recent advances in physical reservoir computing: A review. *Neural Networks* **115**, 100–123 (2019). URL <http://www.sciencedirect.com/science/article/pii/S0893608019300784>.
- [18] Kusumoto, T., Mitarai, K., Fujii, K., Kitagawa, M. & Negoro, M. Experimental quantum kernel machine learning with nuclear spins in a solid. *arXiv e-prints* **arXiv:1911.12021** (2019).
- [19] Ballarini, D. *et al.* Polaritonic neuromorphic computing outperforms linear classifiers. *arXiv e-prints* **arXiv:1911.02923** (2019).
- [20] Fujii, K. & Nakajima, K. Harnessing disordered-ensemble quantum dynamics for machine learning. *Physical Review Applied* **8**, 024030– (2017). URL <https://link.aps.org/doi/10.1103/PhysRevApplied.8.024030>.
- [21] Ghosh, S., Opala, A., Matuszewski, M., Paterek, T. & Liew, T. C. H. Quantum reservoir processing. *npj Quantum Information* **5**, 35 (2019). URL <https://doi.org/10.1038/s41534-019-0149-8>.
- [22] Nielsen, M. A. & Chuang, I. Quantum computation and quantum information. *American Journal of Physics* **70**, 558–559 (2002). URL <https://doi.org/10.1119/1.1463744>.
- [23] Almudever, C. G. *et al.* The engineering challenges in quantum computing. In *The engineering challenges in quantum computing*, 836–845 (Design, Automation & Test in Europe Conference & Exhibition, 2017).
- [24] Arute, F. *et al.* Quantum supremacy using a programmable superconducting processor. *Nature* **574**, 505–510 (2019). URL <https://doi.org/10.1038/s41586-019-1666-5>.
- [25] Chiesa, A. *et al.* Quantum hardware simulating four-dimensional inelastic neutron scattering. *Nature Physics* **15**, 455–459 (2019). URL <https://doi.org/10.1038/s41567-019-0437-4>.
- [26] Fowler, A. G., Mariantoni, M., Martinis, J. M. & Cleland, A. N. Surface codes: Towards practical large-scale quantum computation. *Physical Review A* **86**, 032324– (2012). URL <https://link.aps.org/doi/10.1103/PhysRevA.86.032324>.
- [27] Esslinger, T. Fermi-hubbard physics with atoms in an optical lattice. *An-*

- Annual Review of Condensed Matter Physics* **1**, 129–152 (2010). URL <https://www.annualreviews.org/doi/abs/10.1146/annurev-conmatphys-070909-104059>.
- [28] Hofstetter, W. & Qin, T. Quantum simulation of strongly correlated condensed matter systems **51**, 082001 (2018). URL <http://dx.doi.org/10.1088/1361-6455/aaa31b>.
- [29] Tarruell, L. & Sanchez-Palencia, L. Quantum simulation of the hubbard model with ultracold fermions in optical lattices. *Comptes Rendus Physique* **19**, 365–393 (2018). URL <http://www.sciencedirect.com/science/article/pii/S1631070518300926>.
- [30] Carusotto, I. *et al.* Fermionized photons in an array of driven dissipative nonlinear cavities. *Physical Review Letters* **103**, 033601– (2009). URL <https://link.aps.org/doi/10.1103/PhysRevLett.103.033601>.
- [31] Bardyn, C. E. & Imamoglu, A. Majorana-like modes of light in a one-dimensional array of nonlinear cavities. *Physical Review Letters* **109**, 253606– (2012). URL <https://link.aps.org/doi/10.1103/PhysRevLett.109.253606>.
- [32] Chang, D. E., Vuletić, V. & Lukin, M. D. Quantum nonlinear optics —photon by photon. *Nature Photonics* **8**, 685 (2014). URL <https://doi.org/10.1038/nphoton.2014.192>.
- [33] Angelakis, D. G. *Quantum Simulations with Photons and Polaritons: Merging Quantum Optics with Condensed Matter Physics* (Springer International Publishing, Cham, Switzerland, 2017).
- [34] Vaneph, C. *et al.* Observation of the unconventional photon blockade in the microwave domain. *Physical Review Letters* **121**, 043602– (2018). URL <https://link.aps.org/doi/10.1103/PhysRevLett.121.043602>.
- [35] Delteil, A. *et al.* Towards polariton blockade of confined exciton–polaritons. *Nature Materials* **18**, 219–222 (2019). URL <https://doi.org/10.1038/s41563-019-0282-y>.
- [36] Emmanuele, R. P. A. *et al.* Highly nonlinear trion-polaritons in a monolayer semiconductor. *arXiv:1910.14636* (2019).
- [37] Kyriienko, O., Krizhanovskii, D. N. & Shelykh, I. A. Nonlinear quantum optics with trion-polaritons in 2d monolayers: conventional and unconventional photon blockade. *arXiv:1910.11294* (2019).
- [38] Pierre, T. *et al.* Coherent nonlinear optics of quantum emitters in nanophotonic waveguides. *Nanophotonics* **8**, 1641 (2019). URL <https://www.degruyter.com/view/j/nanoph.2019.8.issue-10/nanoph-2019-0126/nanoph-2019-0126.xml>.
- [39] Roy, D., Wilson, C. M. & Firstenberg, O. Colloquium: Strongly interacting photons in one-dimensional continuum. *Reviews of Modern Physics* **89**, 021001– (2017). URL <https://link.aps.org/doi/10.1103/RevModPhys.89.021001>.
- [40] Fitzpatrick, M., Sundaresan, N. M., Li, A. C. Y., Koch, J. & Houck, A. A. Observation of a dissipative phase transition in a one-dimensional circuit qed lattice. *Physical Review X* **7**, 011016– (2017). URL <https://link.aps.org/doi/10.1103/PhysRevX.7.011016>.
- [41] Nissen, F. *et al.* Nonequilibrium dynamics of coupled qubit-cavity arrays. *Physical Review Letters* **108**, 233603– (2012). URL <https://link.aps.org/doi/10.1103/PhysRevLett.108.233603>.

- [42] Snijders, H. J. *et al.* Observation of the unconventional photon blockade. *Phys. Rev. Lett.* **121**, 043601 (2018). URL <https://link.aps.org/doi/10.1103/PhysRevLett.121.043601>.
- [43] Scarlino, P. *et al.* Coherent microwave-photon-mediated coupling between a semiconductor and a superconducting qubit. *Nature Communications* **10**, 3011 (2019). URL <https://doi.org/10.1038/s41467-019-10798-6>.
- [44] Srednicki, M. *Quantum Field Theory* (Cambridge University Press, Cambridge, 2007). URL <https://www.cambridge.org/core/books/quantum-field-theory/718DD037728FB3745F48A40A6D9A8A1C>.
- [45] Altland, A. & Simons, B. D. *Condensed Matter Field Theory* (Cambridge University Press, Cambridge, 2010). URL <https://www.cambridge.org/core/books/condensed-matter-field-theory/0A8DE6503ED868D96985D9E7847C63FF>.
- [46] Biamonte, J. *et al.* Quantum machine learning. *Nature* **549**, 195 (2017). URL <https://doi.org/10.1038/nature23474>.
- [47] Kutvonen, A., Sagawa, T. & Fujii, K. Recurrent neural networks running on quantum spins: memory accuracy and capacity. *arXiv e-prints* **arXiv:1807.03947** (2018).
- [48] Farhi, E. & Neven, H. Classification with quantum neural networks on near term processors (2018). URL <https://ui.adsabs.harvard.edu/#abs/2018arXiv180206002F>.
- [49] Grant, E. *et al.* Hierarchical quantum classifiers. *npj Quantum Information* **4**, 65 (2018). URL <https://doi.org/10.1038/s41534-018-0116-9>.
- [50] Cong, I., Choi, S. & Lukin, M. D. Quantum convolutional neural networks. *Nature Physics* **15**, 1273–1278 (2019). URL <https://doi.org/10.1038/s41567-019-0648-8>.
- [51] Havlíček, V. *et al.* Supervised learning with quantum-enhanced feature spaces. *Nature* **567**, 209–212 (2019). URL <https://doi.org/10.1038/s41586-019-0980-2>.
- [52] Amin, M. H., Andriyash, E., Rolfe, J., Kulchyskyy, B. & Melko, R. Quantum boltzmann machine. *Physical Review X* **8**, 021050– (2018). URL <https://link.aps.org/doi/10.1103/PhysRevX.8.021050>.
- [53] Banchi, L., Pancotti, N. & Bose, S. Quantum gate learning in qubit networks: Toffoli gate without time-dependent control. *npj Quantum Information* **2**, 16019 (2016). URL <https://doi.org/10.1038/npjqi.2016.19>.
- [54] Zahedinejad, E., Ghosh, J. & Sanders, B. C. Designing high-fidelity single-shot three-qubit gates: A machine-learning approach. *Physical Review Applied* **6**, 054005– (2016). URL <https://link.aps.org/doi/10.1103/PhysRevApplied.6.054005>.
- [55] Yang, X., Li, J. & Peng, X. An improved differential evolution algorithm for learning high-fidelity quantum controls. *Science Bulletin* **64**, 1402–1408 (2019). URL <http://www.sciencedirect.com/science/article/pii/S2095927319304104>.